Letter

Superconducting properties of rare-earth boron hydrides at high pressure studied by first-principles calculations

Simin Li,[1,2] Weiguo Sun,[1] Hanyu Liu,[3,*] Cheng Lu,[4,†] and Feng Peng[1,‡]

[1]*College of Physics and Electronic Information, Luoyang Normal University, Luoyang 471022, China*

[2]*Institute of High Pressure Physics, School of Physical Science and Technology, Ningbo University, Ningbo 315211, China*

[3]*International Center for Computational Method and Software and State Key Lab of Superhard Materials, College of Physics, Jilin University, Changchun 130012, China*

[4]*School of Mathematics and Physics, China University of Geosciences (Wuhan), Wuhan, 430074, China*

(Received 21 April 2023; revised 30 July 2024; accepted 8 August 2024; published 20 August 2024)

It is a long-thought proposal that dense light-element molecular hydrides, such as diborane (B_2H_6) and methane (CH_4), offer an ideal platform to search for phonon-mediated superconductors. However, these hydrides are often unstable under sufficiently high pressure, e.g., B_2H_6 decomposed into BH and H_2 at pressures of above 153 GPa, which are unlikely to exhibit high superconductivity. Here, we find a feasible route to stabilize these light-element molecular hydrides with high superconductivity under high pressure by high-throughput structure searches and first-principles calculations. We uncover a series of stable H-rich rare-earth (R) metal based boron hydrides RB_2H_{10} with polydiborane networks. Strikingly, YB_2H_{10} is predicted to be a high-temperature superconductor with unprecedentedly critical temperature (T_c) of up to 93 K under 150 GPa. The present findings open a route to stabilize the unstable diborane by bringing the additional R metals into the lattice under high pressure, as well as tuning the superconductivity among diborane-based hydrides and other similar dense light-element molecular hydrides.

DOI: 10.1103/PhysRevB.110.L060514

The search for high-T_c superconductivity among hydrogen-rich compounds provides a unique route to discover high- or even room-temperature superconductors due to the creation of pressure-induced atomic hydrogen in the lattice, in which the low mass of hydrogen possesses high Debye temperature and high vibrational frequencies as well as strong electron-phonon coupling [1,2]. Following this concept, numerous studies have been devoted to the investigation of hydrogen-rich compounds under high pressure [3–8], where there has been several breakthrough progress in the system of binary hydrides, such as H_3S with a T_c of 203 K below 200 GPa [9–11] and the R (Sc, Y, La, Ce, Pr, etc.) based hydrides [12,13] with remarkable high T_c and clathrate-like caged networks of hydrogen atoms embedded R atom. Moreover, with the rapid development of theory and experiment techniques, ternary hydrides are also found to become promising candidates for high-T_c superconductors [14–20].

The light-element hydrogen-rich compounds, such as boron or carbon hydride, in principle, should exhibit a relatively high T_c, since these elements with low mass and high Debye temperature, together with pressure-induced metallization, which leads to strong electron-phonon coupling based on Bardeen-Cooper-Schrieffer (BCS) theory. However, these hydrides were not predicted with superior thermodynamical stability under high pressure. For example, diborane (B_2H_6), as a typical molecular crystal with strong covalent bonds, were found to become unstable and decompose into BH and H_2 at 153 GPa [21]. It is natural to ask if there is a feasible way to stabilize this unstable B_2H_6 configuration, especially for tuning it to be a superconductor under high pressure? The recently works have proven that one possible solution is to introduce unsaturation salt, such as the lower oxidation rare-earth hydrides with strong Coulomb interaction and the redundancy valence electrons, forming the steady salt lattice for stabilizing these unstable light-element hydrides under high pressure [22]. High-temperature superconducting hydrides at low pressures have also been found in the La-B-H system, which also suggests that it is feasible to achieve high-temperature superconductivity by the addition of transition metals to the B-H system [23]. To this end, we perform comprehensive exploration of the structural phase diagrams of R (Sc, Y, Ho, Lu, etc.)-based hydrides with H-rich species under high pressure by the CALYPSO structural search method [24,25] and first-principles calculations. As a result, our simulations identify several stable structures of RB_2H_8 and RB_2H_{10}, where the B_2H_6 or BH_4 units are found to become robustly stable in the lattice. Intriguingly, compared with the original B_2H_6, YB_2H_{10} is predicted to become a high-temperature superconductor with the high-T_c value of 93 K, at the same pressure of 150 GPa. These results shed light on the further design and discovery of stabilizing unstable compounds with unique property under high pressure.

We first calculate the formation enthalpies of the predicted structures of RB_2H_n (R = Sc, Y, Ho, and Lu), which are evidenced in the convex hull as shown in Figs. 1(a)–1(d) and Supplemental Material Figs. S1– S4 [26]. The stabilities of

*Contact author: lhy@calypso.cn
†Contact author: lucheng@calypso.cn
‡Contact author: fpeng@calypso.cn

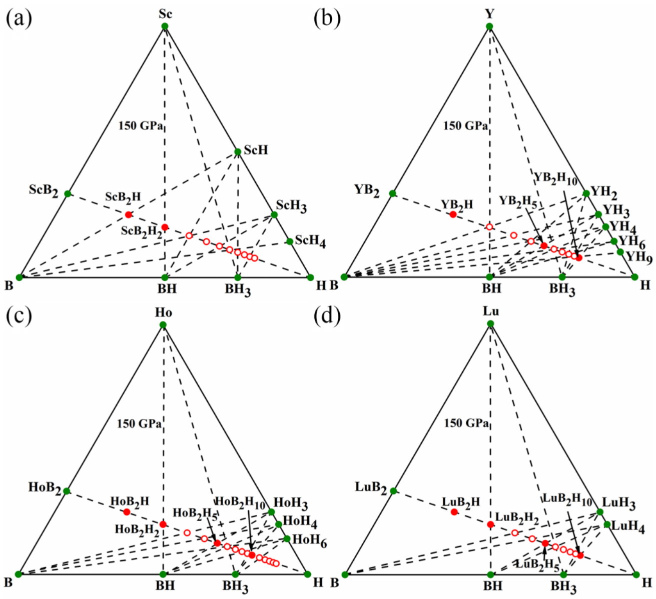

FIG. 1. Trigonal phase diagrams of the *R*–B–H system at 150 GPa. (a) Sc-B-H, (b) Y-B-H, (c) Ho-B-H, and (d) Lu-B-H. Solid red symbols denote the stable stoichiometries of RB_2H_n.

RB_2H_n (R = Sc, Y, Ho, and Lu) are well evaluated by the decomposed chemical reactions with products of RB_2 and H_2, where RB_2 are the most stable *R* diborides at corresponding pressure [51–53]. Supplemental Material Figs. S5(a)– S8(a) [26] show that RB_2H remains stable relative to RB_2 and H atoms in the pressure range of 50–150 GPa for RB_2H_n (R = Sc, Y, Ho and Lu). Besides, RB_2H_2, RB_2H_5, RB_2H_8, RB_2H_{10} hydrides are also found to be thermodynamically stable in the considered pressure range, and the hydrogen contents for the stable stoichiometries are altered by choosing the *R* metals with larger atomic number. Interestingly, for most RB_2-H hydrides, the ground structures are the same symmetries for the same stoichiometries. The calculated stable pressure ranges for various stoichiometries of RB_2-H hydrides are summarized, as shown in Figs. S5(b)– S8(b) [26]. Remarkably, H-richer RB_2H_7 and RB_2H_{10} species exhibiting ideal diborane configurations are unexpectedly predicted, as shown in Figs. 2(c) and 2(d).

In general, zero-point energy (ZPE) plays a critical role in stabilizing the H-rich compounds. We have further investigated the relative stabilities of RB_2H_n (R = Sc, Y, Ho and Lu) considering the ZPE corrections. After the reexamination of the phase transition orders of RB_2H_n (R = Sc, Y, Ho and Lu) by the total energies with and without ZPE corrections at 150 GPa (Fig. S9 and Table S1 [24]), the results indicate that there is almost no change for the phase transition orders of our predicted structures. Moreover, a few phases of RB_2H_n are found to become more stable after considering ZPE corrections.

The planar B layers similar to graphene can be seen in RB_2H and RB_2H_2 hydrides, where RB_2H maintains the $P2_1/m$ structure in all considered pressure ranges, as shown in Fig. 2(a). This structure consists of layered and six-membered B rings and *R*-H chains along the *b* axis, with layers bridged by sharing H atoms. RB_2H_2 (see Fig. S10(a) [26]) possesses

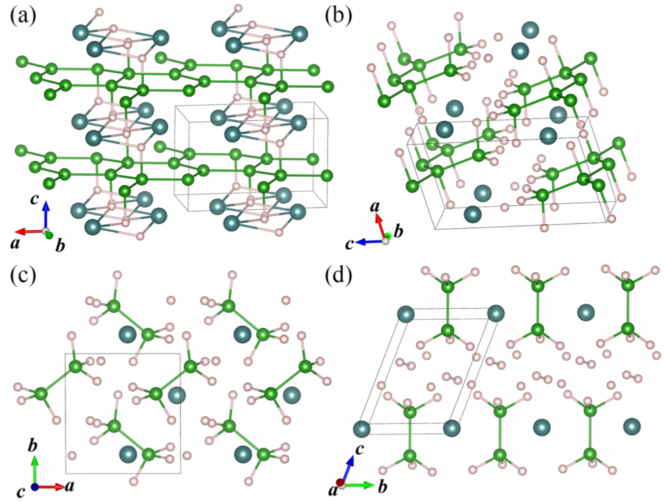

FIG. 2. The predicted crystal structures of the energetically stable RB_2H_n hydrides. (a) $P2_1/m$ phase of RB_2H, (b) $P2_1$ phase of RB_2H_4, (c) *P1* phase of RB_2H_7, (d) *P-1* phase of RB_2H_{10}. The dark green, green, and pink spheres denote *R*, B and H atoms, respectively.

Pmna structure, which can be reviewed as two layers of B-H networks and the *R* metal layer aligned along the *c*-axis direction. With increasing the content of H, the infinite zigzag B-B chains are found in RB_2H_4 and RB_2H_5. RB_2H_4 [see Fig. 2(b)] adopts $P2_1$ structure, this structure can be regarded as the infinite zigzag chains of $\cdots$BH-BH$_3\cdots$ dimerics and puckered *R*-H layers at pressure below 150 GPa. As pressure increases, each H atom (proton) in BH units is bridged with two adjoining B ions, forming the B-H-B ionic bonds. However, the large *R* atoms and the inequivalent charge distributions squeeze the strong B-H-B networks, which eventually cause a puckered plane of B_2H_4. RB_2H_5 is stable with *Pnam* symmetry (see Fig. S10(d) [26]). It is composed of *R*-H chains and infinite zigzag BH_2-BH_2 chains. Interestingly, the B_2H_6 units can be also found in RB_2H_7 and RB_2H_{10}. RB_2H_7 [Fig. 2(c)] is composed of *R* atoms, B_2H_6 and isolated H atoms, by contrast, and RB_2H_{10} [Fig. 2(d)] consists of *R* atoms, H_2 molecules, and B_2H_6 units arranged in layers along the *c* axis. These results motivate us to extend our theoretical calculations to explore whether other *R* atoms can also stabilize the diborane under high pressure. As a consequence, based on the predicted ground state structures database of RB_2H_n (R = Sc, Y, Ho and Lu), our simulations employing a high-throughput calculation on some other *R* (R = Tb, Dy, Er, Tm, Yb, U and Pu) boron hydrides by substitution the *R* atoms into the ground state structures of RB_2H_n (Figs. S11– S22 [26]) show that, unsurprisingly, the B_2H_6 units are emerged in these *R* based boron hydrides. Thus, stabilization of diborane under high pressure by using *R* atoms is an effective avenue to stabilize other light-element molecular compounds, such as H_2O, CH_4, NH_3, etc., under high pressure.

The planar B layers in RB_2H and RB_2H_2 are similar to the B layers in MgB_2 superconductors [54]. However, their superconductivity mechanisms are different from MgB_2, which are mainly contributed by the vibration of BH units. Unfortunately, the calculated T_c of YB_2H_2 at 100 GPa is only 10 K, which is obviously lower than that of MgB_2 and other

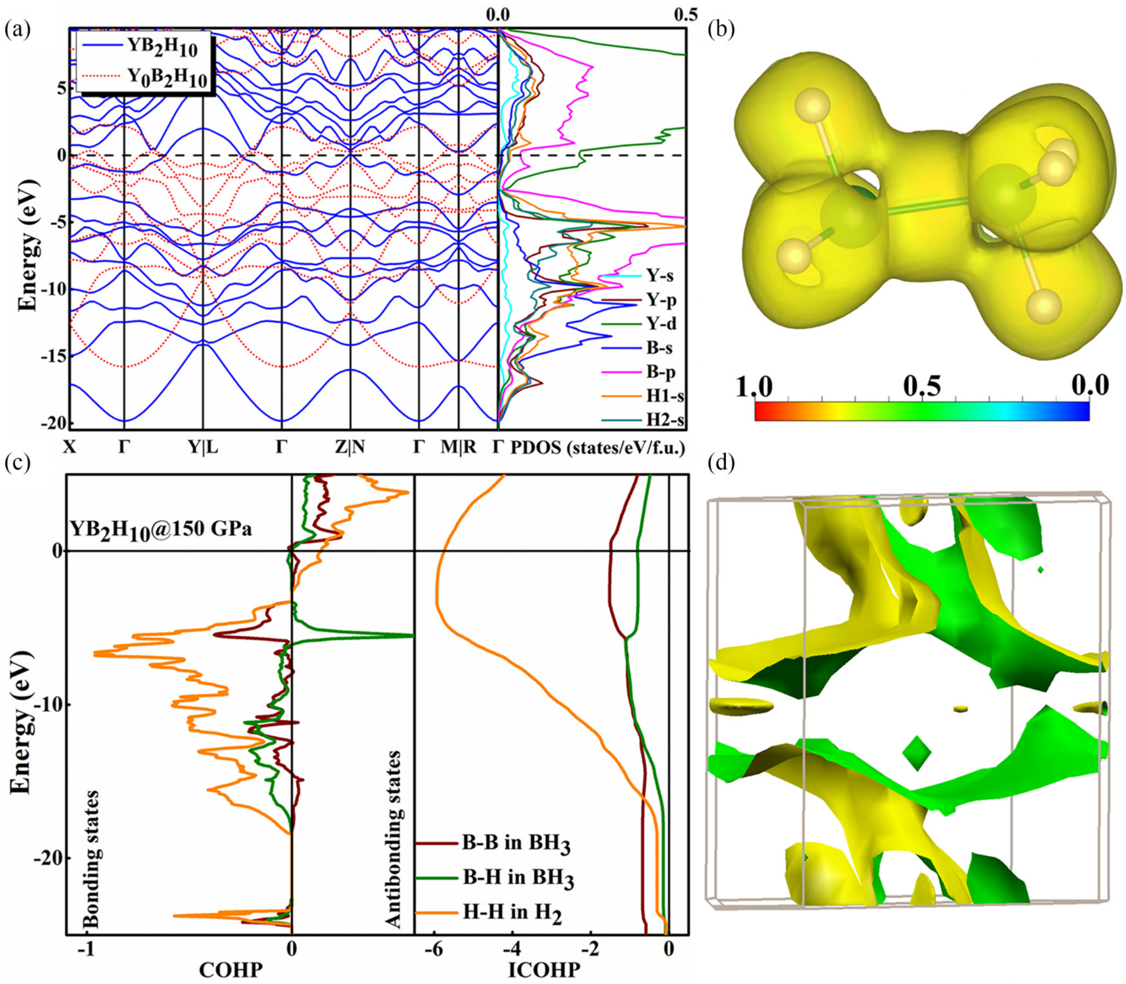

FIG. 3. The electronic properties of YB_2H_{10} at 150 GPa. (a) Energy bands and PDOSs of *P-1* phase of YB_2H_{10} at 150 GPa. In the left panel, the blue solid lines are electronic band structure of YB_2H_{10}. The red dashed lines are those of YB_2H_{10} in which all Y atoms are removed from YB_2H_{10}. The right panel presents the projected DOS of YB_2H_{10}. (b) Electron localization functions of B_2H_6 unit in *P-1* phase of YB_2H_{10}. (c) Calculated COHP and ICHOP of YB_2H_{10}. (d) Calculated Fermi surfaces of YB_2H_{10}.

RB_2H_n compounds containing the BH_3 units. Although the BH_3 structural unit appears in RB_2H_4, unfortunately it is unstable in the energy curves, except for YB_2H_4 and YbB_2H_4 (Figs. S23– S31 [26]). As expected, there are some exceptions, like RB_2H_5 and RB_2H_8, which are stable and also contain BH_3 units, but they are semiconductors due to their ionic character (Figs. S32– S40 [26]). In addition to RB_2H_4 exhibiting metallic properties, we can also see from Fig. 3(a) that YB_2H_{10} shows metallic behavior with bands crossing the Fermi level, and the insertion of Y atoms significantly reduces the band gap of $Y_0B_2H_{10}$, increasing the occupancy of states near the Fermi level, which is beneficial for enhancing the superconducting properties of this system. Here, we do not discuss the physical properties of RB_2H, RB_2H_2, RB_2H_5, and RB_2H_7, but mainly focus on RB_2H_4 ($R = $ Y, Tb and Yb) and RB_2H_{10}.

To examine the chemical bonding of RB_2H_4 and RB_2H_{10}, we calculate the electron localization functions [36] as shown in Figs. S41 [26] and 3(b). Two weakly covalent B-H and B-B chemical bonds are visible through the observed charge localization between B atom and its nearest-neighbor H atoms in BH and BH_3 units for the ground state structure, i.e., the $P2_1$ phase, of YB_2H_4 at 100 GPa. The nearest distances of B-H are 1.36 Å and 1.15 Å in BH and BH_3 units and the B-B separations are 1.6–1.8 Å, which are similar to those in diborane [49]. As for YB_2H_{10} at 100 GPa, the bond lengths of B-H are in the range of 1.14–1.18 Å in BH_3 units, and the B-B bond lengths are 1.61 Å, also similar to those in diborane. To further confirm covalent bonding of B-H and B-B bonds in BH and BH_3 units of YB_2H_4 and YB_2H_{10}, we perform the crystalline orbital Hamiltonian population calculations [55]. The results are shown in Figs. 3(c) and S42 [26], which distinctly reveal the occupancies of B-H and B-B bonding states, supporting for the existence of B-H and B-B covalent bonds in YB_2H_4 and YB_2H_{10}. Moreover, the obvious charge transfer behaviors from R atoms to BH or BH_3 units are observed from the Bader charge analyses [35] (Fig. S43 and Table S2 [26]). The charges on BH or BH_3 units are almost unchanged with the increase of H contents, and the charge values of R atoms are varied from 1.0 e to 1.4 e. Meanwhile, the Fermi surface of YB_2H_{10} at 150 GPa [Fig. 3(d)] shows symmetrically distributed electron pockets up and down near the Y/L point. The strong electron-ion interactions cause the large Madelung energies of the ionic components of R metals

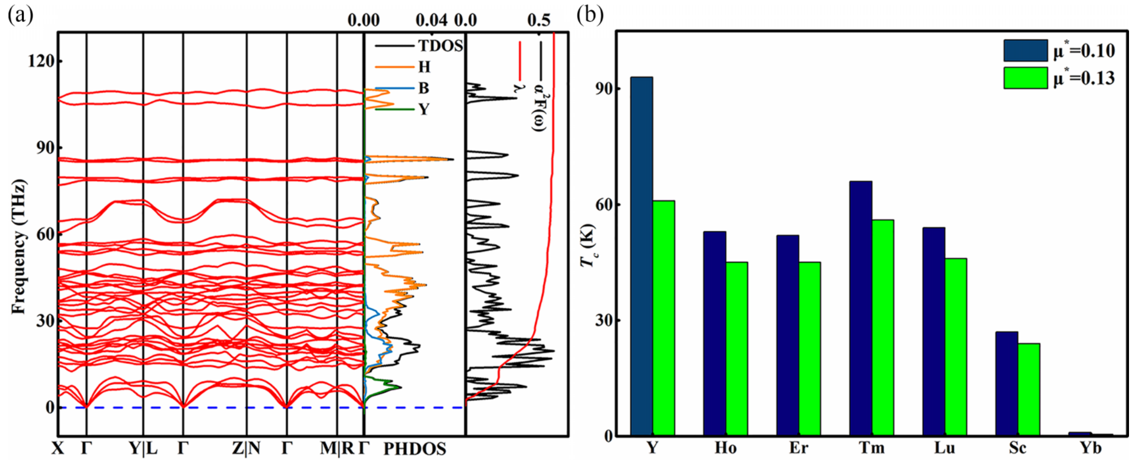

FIG. 4. (a) The phonon dispersion curves, the PHDOS, and the Eliashberg phonon spectral function of $\alpha^2F(\omega)$, and the electron-phonon integral of $\lambda(\omega)$ of the *P-1* phase of YB_2H_{10} at 150 GPa. (b) The calculated T_c of RB_2H_{10} (R = Y, Ho, Er, Tm, Lu, and Yb) at 150 GPa and ScB_2H_{10} at 100 GPa.

and B_2H_6 units, which enhance the stabilities of YB_2H_4 and YB_2H_{10} under high pressure. In addition, the R atoms provide abundant valence electrons to the BH or BH_3 units, which result in the metallic character of BH or BH_3, and eventually induce the superconductivity of RB_2H_4 and RB_2H_{10}.

To explore the thermodynamical mechanisms of R atoms stabilizing the above structures with BH or B_2H_6 units, we take YB_2-H hydride as an example to calculate the internal energies (ΔU), the enthalpies (ΔH), and the pressure-volume term (ΔPV) at 150 GPa. The ΔPV increase with the increasing of H contents, by contrast, the U is decreased as shown in Fig. S44 [26]. The H-rich stoichiometries of YB_2H_4 and YB_2H_{10} containing B_2H_6 units with diborane-type structures tend to become stable and lie on the convex hull.

The calculated electronic band structures and densities of states (DOS) of RB_2H_4 and RB_2H_{10} are shown in Figs. S32–S40 [26]. The electronic DOS at the Fermi level is dominated by the contributions from R atoms, BH and BH_3 units, which indicate the metallic and potential superconductors of RB_2H_4 and RB_2H_{10} with BH and B_2H_6 units. Furthermore, we found that BH and BH_3 units contribute 58% of the total density of states (TDOS) at the Fermi level in YB_2H_4, and BH_3 units contribute 60% in YB_2H_{10}. We then use the Allen-Dynes modified McMillan equation [56] to simulate the superconductivities of RB_2H_4 and RB_2H_{10} containing the B_2H_6 units using the calculated logarithmic average frequency ($\omega_{\log}$) and typical Coulomb pseudopotential parameters (μ^*) from 0.1 to 0.13. The phonon dispersion curves, phonon density of states (PHDOS), and spectral function $\alpha^2F(\omega)$ together with the electron-phonon integral $\lambda(\omega)$ of YB_2H_{10} are shown in Fig. 4(a). For YB_2H_{10}, the EPC calculation yields a moderate λ of 0.68 at 150 GPa, which is benefited from the large B and H-PDOS and high frequency vibrations (above 10 THz) due to the existence of the B_2H_6 units. The simulated T_c values are 93 K (61 K for $(\mu^*) = 0.13$) for YB_2H_{10} at 150 GPa and 21 K [16 K for $(\mu^*) = 0.13$] for YB_2H_4 at 100 GPa, respectively. The calculated T_c of HoB_2H_{10} reaches 53 K using $(\mu^*) = 0.1$ at 150 GPa. Thus, we further investigate the superconductivity of other H-rich compounds containing the B_2H_6 units, as shown in Fig. 4(b). The predicted T_c values of ErB_2H_{10}, TmB_2H_{10}, and LuB_2H_{10} are as high as 52 K, and the calculated T_c values of YB_2H_4 and TbB_2H_4 are about 20 K.

The integration of experimental synthesis with theoretical prediction is crucial for advancing the development of high-temperature superconductors. Recently, the experimental synthesis of LaB_2H_8 [57] high-temperature superconducting hydride has been reported. This aligns with our discussion of the enthalpy of formation of YB_2H_{10} under different pathways, as shown in Figs. S6 and S24 [26]. The optimal synthetic precursors for the experimental synthesis of YB_2H_{10} would be the combination of YB_2H_7 with hydrogen. However, obtaining the initial sample of YB_2H_7 is challenging, as it is a product of YB_2 and hydrogen. Therefore, we could obtain the YB_2 compound through target magnetron sputtering, combine it with ammonia borane, and synthesize YB_2H_{10} using a diamond anvil cell reaction. Alternatively, the same experimental method used for the high-temperature superconducting hydride LaB_2H_8 could be adopted, where the Y and B elements are loaded between diamond anvil cell and prepared by laser heating for high temperature and high pressure reaction.

In summary, we have performed extensively first-principles structure searches on the H-rich R boron hydrides under high pressure. The stabilities and superconductivities of diborane-based compounds with stoichiometry of RB_2H_{10} under high pressure are achieved by the added R atoms. The high-T_c superconductivities of RB_2H_{10} originate from the large electron density of states at the Fermi level derived from B and H atoms and the strong electron-phonon coupling related to the motions of B-H and B-B within molecular diborane. Most importantly, YB_2H_{10} is predicted to be a potential high temperature superconductor with T_c values up to 93 K under 150 GPa. These findings present an effective route to stabilize and metallize diborane under high pressure, which offer key insights for future experiments on synthesis and design of novel high-T_c superconductor.

We acknowledge funding support from the National Natural Science Foundation of China under Grants No. 12174170, No. 12111530103, and No. 12174352. Program for

Excellent Youth Foundation of Henan Scientific Committee (No. 232300421020) and Innovative Research Team (in Science and Technology) in University of Henan Province (No. 24IRTSTHN026).

[1] E. Wigner and H. B. Huntington, On the possibility of a metallic modification of hydrogen, J. Chem. Phys **3**, 764 (1935).
[2] N. W. Ashcroft, Metallic hydrogen: A high-temperature superconductor? Phys. Rev. Lett. **21**, 1748 (1968).
[3] C. J. Pickard, I. Errea, and M. I. Eremets, Superconducting hydrides under pressure, Annu. Rev. Condens. Matter Phys. **11**, 57 (2020).
[4] J. A. Flores-Livas, L. Boeri, A. Sanna, G. Profeta, R. Arita, and M. Eremets, A perspective on conventional high-temperature superconductors at high pressure: Methods and materials, Phys. Rep. **856**, 1 (2020).
[5] A. R. Oganov, C. J. Pickard, Q. Zhu, and R. J. Needs, Structure prediction drives materials discovery, Nat. Rev. Mater. **4**, 331 (2019).
[6] E. Zurek and T. Bi, High-temperature superconductivity in alkaline and rare earth polyhydrides at high pressure: A theoretical perspective, J. Chem. Phys **150**, 050901 (2019).
[7] H. Wang, X. Li, G. Gao, Y. Li, and Y. Ma, Hydrogen-rich superconductors at high pressures, WIREs Comput. Mol. Sci. **8**, e1330 (2018).
[8] L. Zhang, Y. Wang, J. Lv, and Y. Ma, Materials discovery at high pressures, Nat. Rev. Mater. **2**, 17005 (2017).
[9] A. Drozdov, M. Eremets, I. Troyan, V. Ksenofontov, and S. I. Shylin, Conventional superconductivity at 203 kelvin at high pressures in the sulfur hydride system, Nature (London) **525**, 73 (2015).
[10] I. Errea, M. Calandra, C. J. Pickard, J. Nelson, R. J. Needs, Y. Li, H. Liu, Y. Zhang, Y. Ma, and F. Mauri, High-pressure hydrogen sulfide from first principles: A strongly anharmonic phonon-mediated superconductor, Phys. Rev. Lett. **114**, 157004 (2015).
[11] D. Duan, Y. Liu, F. Tian, D. Li, X. Huang, Z. Zhao, H. Yu, B. Liu, W. Tian, and T. Cui, Pressure-induced metallization of dense $(H_2S)_2H_2$ with high-T_c superconductivity, Sci. Rep. **4**, 6968 (2014).
[12] F. Peng, Y. Sun, C. J. Pickard, R. J. Needs, Q. Wu, and Y. Ma, Hydrogen clathrate structures in rare earth hydrides at high pressures: Possible route to room-temperature superconductivity, Phys. Rev. Lett. **119**, 107001 (2017).
[13] H. Liu, I. I. Naumov, R. Hoffmann, N. Ashcroft, and R. J. Hemley, Potential high-T_c superconducting lanthanum and yttrium hydrides at high pressure, Proc. Natl. Acad. Sci. USA **114**, 6990 (2017).
[14] S. Li, H. Wang, W. Sun, C. Lu, and F. Peng, Superconductivity in compressed ternary alkaline boron hydrides, Phys. Rev. B **105**, 224107 (2022).
[15] Y. Yan, T. Bi, N. Geng, X. Wang, and E. Zurek, A metastable $CaSH_3$ phase composed of HS honeycomb sheets that is superconducting under pressure, J. Phys. Chem. Lett. **11**, 9629 (2020).
[16] X. Li, Y. Xie, Y. Sun, P. Huang, H. Liu, C. Chen, and Y. Ma, Chemically tuning stability and superconductivity of P–H compounds, J. Phys. Chem. Lett. **11**, 935 (2020).
[17] P. Zhang, Y. Sun, X. Li, J. Lv, and H. Liu, Structure and superconductivity in compressed Li-Si-H compounds: Density functional theory calculations, Phys. Rev. B **102**, 184103 (2020).
[18] X. Liang, A. Bergara, L. Wang, B. Wen, Z. Zhao, X.-F. Zhou, J. He, G. Gao, and Y. Tian, Potential high-T_c superconductivity in $CaYH_{12}$ under pressure, Phys. Rev. B **99**, 100505(R) (2019).
[19] Y. Sun, J. Lv, Y. Xie, H. Liu, and Y. Ma, Route to a superconducting phase above room temperature in electron-doped hydride compounds under high pressure, Phys. Rev. Lett. **123**, 097001 (2019).
[20] H. Wang, Y. Yao, F. Peng, H. Liu, and R. J. Hemley, Quantum and classical proton diffusion in superconducting clathrate hydrides, Phys. Rev. Lett. **126**, 117002 (2021).
[21] C.-H. Hu, A. R. Oganov, Q. Zhu, G.-R. Qian, G. Frapper, A. O. Lyakhov, and H.-Y. Zhou, Pressure-induced stabilization and insulator-superconductor transition of BH, Phys. Rev. Lett. **110**, 165504 (2013).
[22] F. Peng, Y. Ma, C. J. Pickard, H. Liu, and M. Miao, Universal insertion of molecules in ionic compounds under pressure, Natl. Sci. Rev. **11**, nwae016 (2024).
[23] S. Di Cataldo, S. Qulaghasi, G. B. Bachelet, and L. Boeri, High-T_c superconductivity in doped boron-carbon clathrates, Phys. Rev. B **105**, 064516 (2022).
[24] Y. Wang, J. Lv, L. Zhu, and Y. Ma, Crystal structure prediction via particle-swarm optimization, Phys. Rev. B **82**, 094116 (2010).
[25] Y. Wang, J. Lv, L. Zhu, and Y. Ma, CALYPSO: A method for crystal structure prediction, Comput. Phys. Commun. **183**, 2063 (2012).
[26] See Supplemental Material at http://link.aps.org/supplemental/10.1103/PhysRevB.110.L060514 for computational details, electronic structures, phonon dispersion curves, phase diagrams, and structural parameters of all predicted RB_2-H compounds, which includes Refs. [24,25,27–53].
[27] P. Hohenberg and W. Kohn, Inhomogeneous electron gas, Phys. Rev. **136**, B864 (1964).
[28] W. Kohn and L. J. Sham, Self-consistent equations including exchange and correlation effects, Phys. Rev. **140**, A1133 (1965).
[29] J. P. Perdew, K. Burke, and M. Ernzerhof, Generalized gradient approximation made simple, Phys. Rev. Lett. **77**, 3865 (1996).
[30] J. P. Perdew, J. A. Chevary, S. H. Vosko, K. A. Jackson, M. R. Pederson, D. J. Singh, and C. Fiolhais, Atoms, molecules, solids, and surfaces: Applications of the generalized gradient approximation for exchange and correlation, Phys. Rev. B **46**, 6671 (1992).
[31] G. Kresse and J. Furthmüller, Efficient iterative schemes for ab initio total-energy calculations using a plane-wave basis set, Phys. Rev. B **54**, 11169 (1996).
[32] G. Kresse and D. Joubert, From ultrasoft pseudopotentials to the projector augmented-wave method, Phys. Rev. B **59**, 1758 (1999).

[33] P. E. Blöchl, Projector augmented-wave method, Phys. Rev. B **50**, 17953 (1994).
[34] H. J. Monkhorst and J. D. Pack, Special points for Brillouin-zone integrations, Phys. Rev. B **13**, 5188 (1976).
[35] R. F. W. Bader, Atoms in molecules, Acc. Chem. Res. **18**, 9 (1985).
[36] A. D. Becke and K. E. Edgecombe, A simple measure of electron localization in atomic and molecular systems, J. Chem. Phys **92**, 5397 (1990).
[37] K. Momma and F. Izumi, VESTA 3 for three-dimensional visualization of crystal, volumetric and morphology data, J. Appl. Crystallogr. **44**, 1272 (2011).
[38] A. Togo, F. Oba, and I. Tanaka, First-principles calculations of the ferroelastic transition between rutile-type and $CaCl_2$-type SiO_2 at high pressures, Phys. Rev. B **78**, 134106 (2008).
[39] J. Zheng, W. Sun, X. Dou, A.-J. Mao, and C. Lu, Pressure-driven structural phase transitions and superconductivity of ternary hydride $MgVH_6$, J. Phys. Chem. C **125**, 3150 (2021).
[40] S. Y. Savrasov, Linear-response theory and lattice dynamics: A muffin-tin-orbital approach, Phys. Rev. B **54**, 16470 (1996).
[41] J. Zhao, B. Ao, S. Li, T. Gao, and X. Ye, Phase diagram and bonding states of Pu–H binary compounds at high pressures, J. Phys. Chem. C **124**, 7361 (2020).
[42] W. Zhou, S. Jin, W. Dai, J. T. Lyon, and C. Lu, Theoretical study on the structural evolution and hydrogen storage in NbH_n ($n =$ 2–15) clusters, Int. J. Hydrogen Energy **46**, 17246 (2021).
[43] H. Song, Z. Zhang, T. Cui, C. J. Pickard, V. Z. Kresin, and D. Duan, High T_c superconductivity in heavy rare earth hydrides, Chin. Phys. Lett. **38**, 107401 (2021).
[44] P. Hou, F. Tian, D. Li, B. Chu, Z. Zhao, B. Liu, and T. Cui, High-pressure phase transition of MH_4 (M: Er, Ho), J. Chem. Phys **141**, 054703 (2014).
[45] Y.-L. Hai, Cage Structure and Near Room-Temperature Superconductivity in TbH_n ($n = 1 - 12$), J. Phys. Chem. **125**, 3640 (2021).
[46] I. A. Kruglov, A. G. Kvashnin, A. F. Goncharov, A. R. Oganov, S. S. Lobanov, N. Holtgrewe, S. Jiang, V. B. Prakapenka, E. Greenberg, and A. V. Yanilkin, Uranium polyhydrides at moderate pressures: Prediction, synthesis, and expected superconductivity, Sci. Adv. **4**, eaat9776 (2018).
[47] Q. Zhuang, X. Jin, Q. Lv, Y. Li, Z. Shao, Z. Liu, X. Li, H. Zhang, X. Meng, K. Bao, and T. Cui, Investigation of superconductivity in compressed vanadium hydrides, Phys. Chem. Chem. Phys. **19**, 26280 (2017).
[48] T. Bi, N. Zarifi, T. Terpstra, and E. Zurek, The search for superconductivity in high pressure hydrides, *Reference Module in Chemistry, Molecular Sciences and Chemical Engineering* (Elsevier, 2019).
[49] Y. Yao and R. Hoffmann, BH_3 under pressure: leaving the molecular diborane motif, J. Am. Chem. Soc. **133**, 21002 (2011).
[50] C. J. Pickard and R. J. Needs, Structure of phase III of solid hydrogen, Nat. Phys. **3**, 473 (2007).
[51] M. Zhang, H. Wang, H. Wang, X. Zhang, T. Iitaka, and Y. Ma, First-Principles prediction on the high-pressure structures of transition metal diborides (TMB_2, TM= Sc, Ti, Y, Zr), Inorg. Chem. **49**, 6859 (2010).
[52] F. Ling, K. Luo, L. Hao, Y. Gao, Z. Yuan, Q. Gao, Y. Zhang, Z. Zhao, J. He, and D. Yu, Universal phasetransitions of AlB_2-type transition-metal diborides, ACS Omega **5**, 4620 (2020).
[53] G. Akopov, M. T. Yeung, and R. B. Kaner, Rediscovering the crystal chemistry of borides, Adv. Mater. **29**, 1604506 (2017).
[54] Y. Ma, Y. Wang, and A. R. Oganov, Absence of superconductivity in the high-pressure polymorph of MgB_2, Phys. Rev. B **79**, 054101 (2009).
[55] V. L. Deringer, A. L. Tchougréeff, and R. Dronskowski, Crystal orbital Hamilton population (COHP) analysis as projected from plane-wave basis sets, J. Phys. Chem. A **115**, 5461 (2011).
[56] P. Giannozzi, S. Baroni, N. Bonini, M. Calandra, R. Car, C. Cavazzoni, D. Ceresoli, G. L. Chiarotti, M. Cococcioni, I. Dabo, A. Dal Corso, S. de Gironcoli, S. Fabris, G. Fratesi, R. Gebauer, U. Gerstmann, C. Gougoussis, A. Kokalj, M. Lazzeri, L. Martin-Samos, N. Marzari *et al.*, QUANTUM ESPRESSO: A modular and open-source software project for quantum simulations of materials, J. Phys.: Condens. Matter **21**, 395502 (2009).
[57] X. Song, X. Hao, X. Wei, X.-L. He, H. Liu, L. Ma, G. Liu, H. Wang, J. Niu, S. Wang, Y. Qi, Z. Liu, W. Hu, B. Xu, L. Wang, G. Gao, and Y. Tian, Superconductivity above 105 K in nonclathrate ternary lanthanum borohydride below megabar pressure, J. Am. Chem. Soc. **146**, 13797 (2024).